

Solvent Accessibility in the Distal Heme Pocket of the Nitrosyl d₁-Heme Complex of *Pseudomonas stutzeri* cd₁ Nitrite Reductase

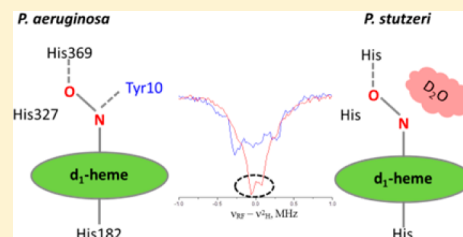
Marina Radoul,[†] Yoav Barak,[#] Serena Rinaldo,[§] Francesca Cutruzzolà,[§] Israel Pecht,[‡] and Daniella Goldfarb^{*,†}

[†]Departments of Chemical Physics and [‡]Immunology, [#]Nanobio Lab, Weizmann Institute of Science, Israel

[§]Istituto Pasteur-Fondazione Cenci Bolognetti, Department of Biochemical Sciences, Sapienza University of Rome, Rome, Italy

Supporting Information

ABSTRACT: In nitrite reductase (cd₁ NIR), the c-heme mediates electron transfer to the catalytic d₁-heme where nitrite (NO₂[−]) is reduced to nitric oxide (NO). An interesting feature of this enzyme is the relative lability of the reaction product NO bound to the d₁-heme. Marked differences in the c- to d₁-heme electron-transfer rates were reported for cd₁ NIRs from different sources, such as *Pseudomonas stutzeri* (*P. stutzeri*) and *Pseudomonas aeruginosa* (*P. aeruginosa*). The three-dimensional structure of the *P. aeruginosa* enzyme has been determined, but that of the *P. stutzeri* enzyme is still unknown. The difference in electron transfer rates prompted a comparison of the structural properties of the d₁-heme pocket of *P. stutzeri* cd₁ NIR with those of the *P. aeruginosa* wild type enzyme (WT) and its Y10F using their nitrosyl d₁-heme complexes. We applied high field pulse electron paramagnetic resonance (EPR) techniques that detect nuclear spins in the close environment of the spin bearing Fe(II)-NO entity. We observed similarities in the rhombic g-tensor and detected a proximal histidine ligand with ¹⁴N hyperfine and quadrupole interactions also similar to those of *P. aeruginosa* WT and Y10F mutant complexes. In contrast, we also observed significant differences in the H-bond network involving the NO ligand and a larger solvent accessibility for *P. stutzeri* attributed to the absence of this tyrosine residue. For *P. aeruginosa*, cd₁ NIR domain swapping allows Tyr₁₀ to become H-bonded to the bound NO substrate. These findings support a previous suggestion that the large difference in the c- to d₁-heme electron transfer rates between the two enzymes is related to solvent accessibility of their d₁-heme pockets.



Cytochrome cd₁ nitrite reductase (NIR) is one of the key enzymes in the denitrification cycle, which catalyzes the reduction of nitrite to nitric oxide.^{1,2} The most studied cd₁ NIRs are those from *Pseudomonas aeruginosa*³ (*P. aeruginosa*) and *Paracoccus pantotrophus*⁴ (*P. pantotrophus*). The enzyme is a periplasmic homodimer that contains one c-heme and one d₁-heme per monomer.^{4,5} The c-heme takes up electrons and transfers them internally to the d₁-heme, where the nitrite reduction occurs.^{6,7} One of the intriguing aspects of these enzymes is that the nitrite reduction product NO was recently shown to dissociate from the ferrous d₁-heme at rates that are 2–3 orders of magnitude faster than expected.⁸ NO is known to bind with rather high affinity to other types⁹ of ferrous hemes. Because of this relative NO lability, no product inhibition of the enzyme is observed. These findings lead to a modified catalytic mechanism of cd₁ NIRs¹⁰ under conditions of excess reducing equivalents with the following features: (i) The c-heme mediates electron transfer to the d₁-heme from an external electron donor; (ii) nitrite is reduced to NO by the d₁-heme; (iii) the d₁-heme is then reduced again by the c-heme, causing the NO dissociation from the d₁-heme.¹¹ The unexpected fast NO dissociation was attributed to the unique structure of the d₁-heme.^{8,11}

The three-dimensional (3D) structures of WT *P. aeruginosa* cd₁ NIR^{3,12} and *P. pantotrophus* cd₁ NIR¹³ were determined in

the oxidized, reduced, and reduced NO-bound states. In the oxidized state of the *P. aeruginosa* enzyme, “domain swapping” was observed: the N-terminus tail of one monomer crosses the interface between the two subunits, wraps around the other monomer, and places Tyr₁₀ at an H-bond distance from the axial OH[−] ligand of its d₁-heme. In addition, two conserved histidines residues are in the distal pocket of the d₁-heme, His₃₆₉ and His₃₂₇. The histidine to alanine, H327A and H369A mutation of the *P. aeruginosa*, dramatically diminished the nitrite reductase activity.¹⁴ In contrast, replacing Tyr₁₀ with phenylalanine (Y10F) did not affect the enzyme’s activity.¹⁵ Crystal structures of reduced and reduced NO-bound WT enzyme revealed the absence of the hydroxide ion axial ligand and a displacement of the Tyr₁₀ side chain away from the position adopted in the oxidized form.³ Interestingly, the crystal structures of the H327A and H369A¹⁶ mutants exhibit a distortion of the N-terminus and the absence of “domain swapping.” Both mutants share an “open conformation” through which the d₁-heme is more accessible to the solvent than in the WT.

Received: August 20, 2012

Revised: October 12, 2012

Published: October 16, 2012



cd₁ NIR has also been isolated from *Pseudomonas stutzeri* ZoBell (*P. stutzeri*),¹⁷ but its 3D structure has not yet been determined.¹⁸ The cd₁ NIRs of *P. stutzeri* and *P. aeruginosa* share nine homologous histidine residues, yet the major difference between them is the absence of 26 amino acids in the N-terminus of *P. stutzeri* cd₁ NIR.¹⁹ This part of the N-terminus tail is of special interest because it is involved in the domain swapping observed in *P. aeruginosa* cd₁ NIR. It is notable that the missing amino acids include a tyrosine residue equivalent to Tyr₁₀ in *P. aeruginosa* cd₁ NIR. Furthermore, MCD and EPR spectroscopy data have shown that the c-heme has His/Met ligation and the d₁-heme His/hydroxide, as in the oxidized *P. aeruginosa* cd₁ NIR.²⁰ The internal electron-transfer (ET) between the c and d₁ hemes in cd₁ NIRs is an essential step in their catalytic cycle. Interestingly, studies of both *P. aeruginosa* and *P. stutzeri* enzymes showed remarkable differences in the internal ET rates while resolving the fact that both were subject to allosteric control.²¹

Knowledge of solution electronic and geometric structures of the different cd₁ NIRs and their mutants and ligand complexes is essential for understanding the aforementioned distinct reactivity. This work specifically attempts to address the nature of the nitrosyl d₁-heme complex as a step toward understanding the origin of the relatively fast NO dissociation rate.¹¹ Using myoglobin as a reference system, we recently demonstrated that high field pulse EPR (W-band, 95 GHz, ~3.5 T), combined with density functional theory (DFT) calculations, is a highly effective methodology for identifying and characterizing H-bonds between the amino acid residues in the distal heme pocket and the NO. In addition, it allows characterizing the coordination of the nitrogen of the axial histidine ligand.²² We then applied this methodology to characterize the nitrosyl d₁-heme complexes of WT and two mutants, Y10F and H369A/H327A (where both His₃₆₉ and His₃₂₇ were replaced with alanine), of *P. aeruginosa* cd₁ NIR.^{23,24} We showed that the NO moiety in the nitrosyl d₁-heme forms H-bonds with Tyr₁₀ and His₃₆₉, whereas His₃₂₇ appears to be less involved in H-bonding to NO. This contrasts with the 3D crystal structure in which Tyr₁₀ is shifted away from the NO.¹⁶ We also observed that these mutations increase solvent accessibility to the distal pocket. Moreover, the H-bonding network within the active site of *P. aeruginosa* cd₁ NIR was shown to be highly dynamic with a cooperative behavior of the residues in the distal pocket. In Y10F, His₃₆₉ comes closer to the bound NO, whereas mutation of both distal histidines (H369A/H327A) severs the H-bond of Tyr₁₀.²⁴

The present study focuses on the nitrosyl d₁-heme complex of *P. stutzeri* cd₁ NIR and compares its EPR parameters with those obtained previously for the *P. aeruginosa* enzyme. Such a comparison is highly relevant in light of the differences observed in the internal ET rates and the absence of the Tyr in the distal pocket of the *P. stutzeri* enzyme. As in our previous studies,^{22–24} the measurements were carried out at W-band frequencies, benefit from higher spectral resolution, and require considerably smaller protein amounts. This is particularly important for cd₁ NIR, which cannot be expressed in *E. coli* given its inability to produce d₁-heme. In addition, we developed a faster, easier, and good yield purification protocol.²⁵ We found the same binding characteristics of the proximal histidine to the Fe(II) in the two enzymes as manifested by the coordinated ¹⁴N hyperfine and quadrupolar interactions. This finding suggests that the distal pocket of the active site is responsible for the variations observed in ET rates.

The significant structural differences observed were in the H-bond network to N(NO) attributable to the absent tyrosine residue in the N-terminus of *P. stutzeri* cd₁ NIR. Remarkably, the ¹H/²H ENDOR (electron-double nuclear resonance) spectra of the nitrosyl d₁-heme from *P. stutzeri* cd₁ NIR revealed high similarity to those of the Y10F mutant of the *P. aeruginosa* enzyme. This similarity allowed us to assign the largest observed couplings to an H-bond from one of the conserved histidines in the distal pocket of the active site of *P. stutzeri* cd₁ NIR. The absence of the tyrosine residue in the distal pocket also leads to larger solvent accessibility, which supports the earlier interpretation of the differences in ET transfer rates.

MATERIALS AND METHODS

Enzyme Purification. *P. Stutzeri* cd₁ NIR was purified using a method similar to that reported earlier for *P. aeruginosa* cd₁ NIR²⁷ and *P. stutzeri* cd₁ NIR^{20,25} with the following modifications.²⁸ Because cd₁ NIR is a periplasmic enzyme, lysis of the outer membrane was performed. The *P. stutzeri* cells were resuspended at a ratio of 100 g/L in the lysis buffer (0.5 M sucrose, 3 mM EDTA, 100 mM Tris pH 8.0, and 700 mg/L of lysozyme) and incubated at 30 °C for 60 min and shaken at 50 rpm. The suspension was centrifuged at 24000g for 1 h. The pellet was discarded and the supernatant was saturated with (NH₄)₂SO₄. The precipitate was collected through centrifugation, dissolved in 10 mM Tris pH 7.5, and centrifuged again. The supernatant was diluted to a conductivity less than 5 mS/cm, loaded onto the DEAE-cellulose column equilibrated with 10 mM Tris, pH 7.5, and eluted with a linear gradient 0–400 mM KCl in 10 mM Tris pH 7.5 (isoelectric point of *P. stutzeri* cd₁ NIR is 6.5).^{17,29} The fractions absorbing at 640 nm were combined and dialyzed against 50 mM Tris pH 7.0. The concentrated sample was then loaded onto a G75 (Sephadex column) equilibrated with 50 mM Tris pH 7.5. The fractions absorbing at 640 nm were pooled and loaded onto DEAE equilibrated with 10 mM Tris pH 7.5 and eluted with a linear gradient 0–400 mM KCl in 10 mM Tris pH 7.5. Nitrite reductase was eluted in two clearly distinguishable peaks. The two fractions absorbing at 640 nm were dialyzed separately against 10 mM KH₂PO₄ pH 5.0, and each fraction was loaded onto the CM column equilibrated with 10 mM KH₂PO₄ pH 5.0. The fractions were eluted with a linear gradient to 50 mM KH₂PO₄ pH 7.2. The purity of the protein was evaluated spectrophotometrically from the A₄₁₁/A₂₈₀ ratio = 1.2 and by SDS-PAGE. The fractions with the ratio A₄₁₁/A₂₈₀ = 1.2 were pooled together (ϵ_{411} = 282 mM⁻¹ cm⁻¹). Figure S1 in the Supporting Information (SI) presents the purification steps as revealed by silver stained SDS-PAGE, where the band at ~60 kDa corresponds to the molecular mass per one monomer of cd₁ NIR *P. stutzeri*. The presence of two heme groups, c and d₁, in the purified oxidized cd₁ NIR was confirmed by its absorption spectrum (see Figure S2A, SI), and X-band CW EPR spectrum. The observed EPR signals correspond to the g-values, which are similar to those reported previously^{20,30} (see Figure S2B, SI). The total yield of cd₁ NIR from 65 g of *P. stutzeri* cells was 30 mg.

Sample Preparation. The nitrosyl d₁-heme complex of WT *P. stutzeri* cd₁ NIR was prepared under anoxic conditions through sequential addition of sodium ascorbate (~60 mM) and sodium nitrite (~15 mM) to the enzyme in 50 mM phosphate buffer, pH 7.0, yielding a final concentration ~0.3 mM of the complex.³¹ The reduction and NO binding were

monitored using UV–vis absorbance spectroscopy (see Figure 2) on a ~100-fold diluted sample. Shifts in the characteristic d₁-

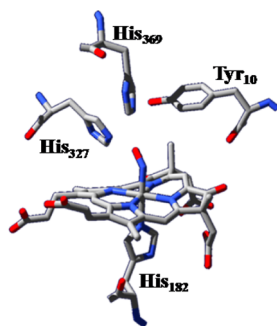


Figure 1. Nitrosyl d₁-heme complex of *P. aeruginosa* cd₁ NIR (PDB: 1nno).

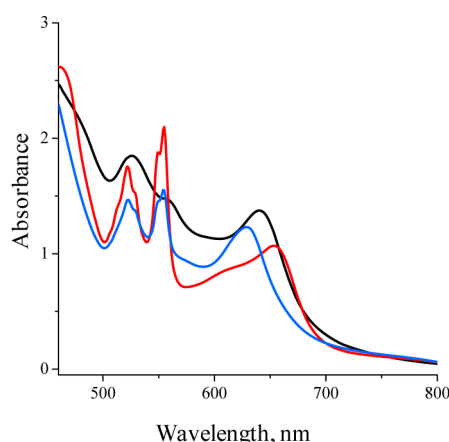


Figure 2. UV–vis absorption spectra of purified *P. stutzeri* cd₁ NIR: oxidized (black), reduced (red), and NO-bound (blue) derivatives.

heme peaks were observed, whereas those of the c-heme shifted upon reduction, but remained unchanged upon NO binding. Glycerol was added (20% of the final volume) for a good glass formation upon freezing. After mixing the components, quartz capillaries (0.6 mm internal diameter, 0.84 mm external diameter) were rapidly filled and frozen by immersing them into liquid nitrogen. The nitrosyl d₁-heme complexes of *P. aeruginosa* cd₁ NIR and its mutants were prepared as described previously.²⁴

Samples Preparation in D₂O. For the deuterium exchange, D₂O (D, 99.9%) and glycerol-(O-d)₃ (D, 98%), both from Cambridge Isotope Laboratories, Inc., were used. The 50 mM phosphate buffer was prepared in D₂O, and 20% of glycerol (by volume) was added. The stock solutions of sodium ascorbate and sodium nitrite were prepared in mixtures of D₂O buffer with deuterated glycerol. All solutions were deaerated by bubbling Argon through them. The initial protein solution was 10-fold diluted using the deuterated buffer/deuterated glycerol mixture and then concentrated. Sodium ascorbate (~60 mM) was added to the concentrated D₂O exchanged protein and incubated for 1 h. Sodium nitrite (~15 mM) was then added in order to give a final concentration of cd₁ NIR ~ 0.3 mM. Quartz capillaries were then filled and samples were immediately frozen in liquid nitrogen. All of these procedures were carried out under anoxic conditions.

Spectroscopic Measurements. X-band continuous wave (CW) EPR spectra were measured on a Bruker Elexsys 500 spectrometer with a power of 25 mW, modulation amplitude = 1 G, time constant = 0.6 s, and microwave frequency ~9.44 GHz, *T* = 130 K.

All pulse EPR measurements were carried out on a home-built W-band (94.9 GHz) spectrometer described elsewhere.³² The temperature for all measurements was 8 K, unless stated otherwise. Field swept echo detected (FS-ED) EPR spectra were recorded using the two-pulse echo sequence, $\pi/2 - \tau - \pi - \tau - \text{echo}$ with $\pi/2$ and π pulse lengths of 12.5 and 25 ns, respectively. FS-ED EPR spectra were simulated using EasySpin.^{33,34} The magnetic field was calibrated using the ¹H Larmor frequency obtained from the ENDOR measurements.

¹H ENDOR spectra were recorded out using the Davies ENDOR³⁵ pulse sequence, $\pi - T - \pi/2 - \tau - \pi - \tau - \text{echo}$, with a radio frequency (RF) π pulse applied during the time interval *T*. The spectra were recorded with τ = 500 ns and $\pi/2$ and π pulses of 100 and 200 ns, respectively. The RF pulse length, *t*_{RF}, was 25 μ s. The ²H ENDOR spectra were recorded using the Mims ENDOR³⁶ sequence $\pi/2 - \tau - \pi/2 - T - \pi/2 - \tau - \text{echo}$, which is better suited than the Davies ENDOR sequence for measurements of small hyperfine couplings. The experiments were conducted with $\pi/2$ pulse duration of 20 ns, *t*_{RF} = 45 μ s, and τ = 400 ns. This τ value places the blind spots well outside the spectral range. In all ENDOR measurements, the echo intensity was measured as a function of the radiofrequency, the repetition time was 10 ms, and 30 shots were collected for each RF setting per one scan. To eliminate baseline distortion, all ENDOR spectra were recorded using random acquisition mode.³⁷ The total number of scans varied from 300 to 10 000 depending on the S/N ratio.

The ENDOR effect, ϵ , for both Davies and Mims ENDOR is defined by

$$\epsilon = [I(RF_{\text{off}}) - I(RF_{\text{on}})]/I(RF_{\text{off}}) \quad (1)$$

¹⁴N HYSORE (hyperfine sublevel correlation) measurements were performed using the pulse sequence $\pi/2 - \tau - \pi/2 - t_1 - \pi - t_2 - \pi/2 - \tau - \text{echo}$.³⁸ The spectra were measured using $\pi/2$ and π pulses of 16 and 32 ns, respectively. The τ value varied between 180 and 220 ns to reduce an effect of blind spots. The dwell time was set to 16 ns and four-phase cycling was employed. The total number of points in each dimension varied from 120 to 140.

The HYSORE data were processed with an *in-house* Matlab program. The background decay in both *t*₁ and *t*₂ dimensions was removed using second-order polynomial fit, followed by apodization with a sine-bell window and zero filling to 512 points in each dimension. A Fourier transform was then carried out in the two dimensions and the magnitude spectrum was calculated.

Theoretical Background. The first-order expression for ¹H ENDOR frequencies is

$$\nu_{\text{ENDOR}}^{\pm} = |\nu_1 \pm A/2| \quad (2)$$

where \pm refers to the different electron manifolds, *A* is the orientation-dependent hyperfine coupling, and ν_1 is the nuclear Larmor frequency. This first-order expression holds when $\nu_1 \gg A$, as usually encountered for ¹H at W-band (~3T) where $\nu_1 \sim 145$ MHz.

For nuclei with *I* > 1/2, the nuclear frequencies additionally depend on the nuclear quadrupole interaction. The ENDOR frequencies of a nucleus with spin *I* = 1, such as ¹⁴N or ²H are

Table 1. Summary of the Peaks Appearing in the UV-Vis Spectra of cd₁ NIR Purified from *P. stutzeri* and *P. aeruginosa* at Oxidized, Reduced, and NO-Bound States and Their Assignments

	λ (oxidized state), nm	λ (reduced state), nm	λ (NO-bound state), nm	ref
<i>P. aeruginosa</i>				
c-heme	520, 550	521, 554, 549/554	525 525, 560	31, 39–41 42
d ₁ -heme	640	625–655	630 635	31, 39–41, 43 42
<i>P. stutzeri</i>				
c-heme	525 525, 555	522, 548/554 522, 550/555	522, 550/555 522, 550/555	25, 28, 39 this work
d ₁ -heme	641 641	625–655 617–653	625–650 630	25, 28, 39 this work

$$\nu_{sq1}^{\pm} = \frac{1}{2}A \pm \nu_1 + \frac{3}{2}P \quad (3)$$

$$\nu_{sq2}^{\pm} = \frac{1}{2}A \pm \nu_1 - \frac{3}{2}P \quad (4)$$

$$\nu_{sq1} + \nu_{sq2} = \nu_{dq} \quad (5)$$

where ν_{sq1} and ν_{sq2} correspond to single quantum nuclear transitions and ν_{dq} corresponds to the double quantum transition. P represents the orientation-dependent quadrupole coupling. The quadrupole splitting within each electron manifold is given by $3P$.

When the magnetic field is along the z principal axes of the quadrupole interaction, $P = P_{zz}$ and is given by

$$P_{zz} = \frac{3e^2Qq}{4hI(2I - 1)} \text{ and } \eta = \frac{P_{xx} - P_{yy}}{P_{zz}} \quad (6)$$

where e^2Qq/h is the so called quadrupole coupling constant.

If the cancellation condition³⁸ $\nu_1 \sim A/2$ holds, the effective field for one of the electron manifolds is zero and the corresponding nuclear transitions become close to the nuclear quadrupole resonance (NQR) frequencies. These frequencies are referred as ν_0 , ν_- , and ν_+ and are expressed by

$$\nu_0 = 2K\eta \quad (7)$$

$$\nu_- = K(3 - \eta) \quad (8)$$

$$\nu_+ = K(3 + \eta) \quad (9)$$

where $\nu_0 + \nu_- = \nu_+$ and $K = (e^2Qq/4h)$

RESULTS

The UV-vis spectra of *P. Stutzeri* cd₁ NIR in the oxidized, reduced, and reduced NO-bound states are shown in Figure 2. Upon reduction, by addition of excess sodium ascorbate, the peaks assigned to the c-heme slightly shift from 525/555 nm to 522/555 nm. Because the c-heme does not react with NO at pH 7.0, the peaks remain at the same position.³¹ In contrast, the peak assigned to the d₁-heme shifts from 640 to 655 nm upon reduction. After addition of sodium nitrite, it further shifts to 630 nm, confirming the formation of the nitrosyl d₁-heme complex.³¹ The peaks assignment and comparison with those obtained previously for the enzyme isolated from *P. stutzeri* and *P. aeruginosa* are presented in Table 1.

EPR Spectra. Figure 3A shows a comparison of the X-band continuous wave (CW) EPR spectrum of a frozen solution of the nitrosyl d₁-heme complex of WT (WT-NO) *P. stutzeri* with those of *P. aeruginosa* WT enzyme and the Y10F mutant

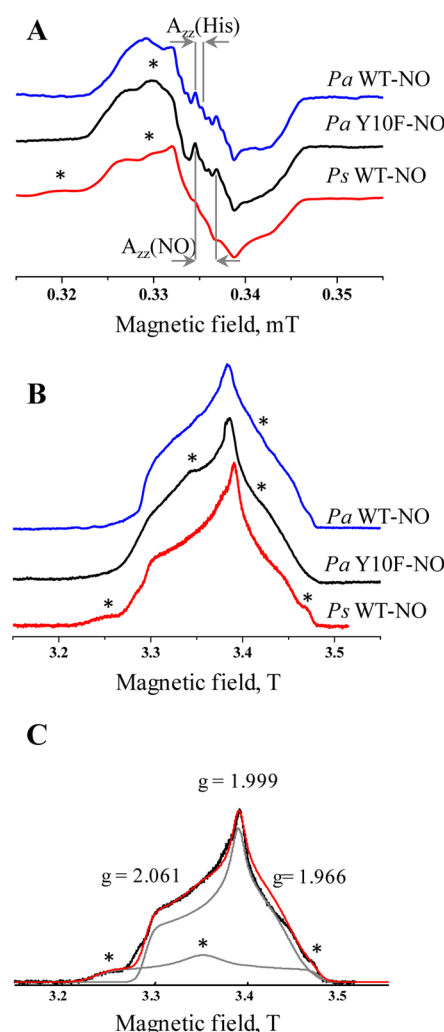


Figure 3. (A) X-band CW EPR spectra of *P. stutzeri* WT-NO (*Ps* WT-NO, red), *P. aeruginosa* WT-NO (*Pa* WT-NO, blue), and Y10F-NO (*Pa* Y10F, black) recorded at 130 K. (B) Same as in A, W-band FS-ED EPR spectra recorded at 8 K. (C) Simulations of the W-band FS-ED EPR spectrum of *P. stutzeri* WT-NO (black). The total simulation (red) comprises the rhombic conformation (gray) and a minor contribution of a second rhombic species (gray) marked with an asterisk (*). The simulation parameters are given in Table 2 and the text.

(Y10F-NO).²⁴ All spectra are governed by a major species with a rhombic g -tensor. Contributions of different minor species are also detectable, particularly in the spectrum of *P. stutzeri* WT-

NO (see Figure 3A). In addition, slight shifts occurred in the g_{zz} (g_{mid}) and g_{yy} (g_{min}) values. ^{14}N hyperfine couplings of the NO are resolved along the g_{zz} direction in all three spectra, but those of the proximal histidine are resolved only in the spectra of *P. aeruginosa* WT-NO and Y10F-NO samples. The exact g -values can be better determined from FS-ED W-band spectra shown in Figure 3B. The dominance of a rhombic species is clear in all samples. As observed in the X-band CW spectra (see Figure 3A), the spectrum of *P. stutzeri* WT-NO exhibits larger g_{zz} and g_{yy} values. A manual best-fit simulation of *P. stutzeri* WT-NO suggests the presence of at least two paramagnetic species with a rhombic g (see Figure 3C). The major species ($\sim 78.5\%$) has g -values of $[g_{xx}, g_{yy}, g_{zz}] = [2.061, 1.966, 1.999]$, whereas the minor species has g -values of $[g_{xx}, g_{yy}, g_{zz}] = [2.095, 2.023, 1.951]$. Similar minor rhombic species were also present in the *P. aeruginosa* WT-NO and Y10F-NO samples.²⁴ As reported previously,²³ different preparations affect the relative amount of the minor species, which is, nevertheless, always low. Table 2 compares the principal g -values of the major species with those of *P. aeruginosa* WT-NO and Y10F-NO.

Table 2. Comparison of the Principal g -values and Hyperfine and Quadrupole Coupling Constants (MHz) of the ^{14}N of the Proximal Histidine and NO for Several Nitrosyl-Heme Complexes, Obtained by Different EPR Techniques

	<i>P. aeruginosa</i> WT-NO	<i>P. aeruginosa</i> Y10F-NO	<i>P. stutzeri</i> WT-NO	myoglobin Mb-NO
g_{min}	1.960 ²⁴	1.970 ²⁴	1.966 ^b	1.987 ²²
g_{mid}	2.004 ²⁴	2.003 ²⁴	1.999	2.008 ²²
g_{max}	2.062 ²⁴	2.062 ²⁴	2.061	2.075 ²²
$A_{\text{min}} (^{14}\text{N}_{\text{His}})$	16.1 ^{24a}	16.1 ²⁴	16.1	17.0 ²²
$A_{\text{mid}} (^{14}\text{N}_{\text{His}})$	16.3 ²⁴	16.3 ²⁴	16.3	17.3 ²²
$A_{\text{max}} (^{14}\text{N}_{\text{His}})$	20.4 ²⁴	20.4 ²⁴	20.4	21.5 ²²
$a_{\text{iso}} (^{14}\text{N}_{\text{His}})$	17.6 ²⁴	17.6 ²⁴	17.6	18.6 ²²
e^2Qq/h	-2.35^{24}			2.6 ²²
$A_{\text{min}} (^{14}\text{N}_{\text{NO}})$		26.9 ²³		
$A_{\text{mid}} (^{14}\text{N}_{\text{NO}})$		33.5 ²³		30.6 ⁴⁴
$A_{\text{max}} (^{14}\text{N}_{\text{NO}})$	66.6	64.5 ²³	62.7	59.9 ⁴⁴
$a_{\text{iso}} (^{14}\text{N}_{\text{NO}})$		41.6 ²³		

^aIn ref 23, the reported hyperfine coupling (A) values were $\pm (16.0, 19.5, 19.5) \pm 0.1$ MHz. The overestimated A_{yy} arose from an incorrect assumption regarding the g -tensor orientation with respect to the heme. The correct orientation was determined later by DFT and confirmed experimentally.²² ^bThe estimated error of the g -values is ± 0.002 and for the hyperfine couplings ± 0.1 MHz.

^1H Davies ENDOR. Well-resolved g -anisotropy at the W-band allowed us to perform orientation selective $^1\text{H}/^2\text{H}$ ENDOR measurements that reveal H-bonded protons to the NO. When discussing orientation selective ENDOR spectra of *P. stutzeri* WT-NO, we should consider the contribution of the minor species, which is 21.5%. The relative contribution of the minor species to the ENDOR spectrum is determined by its relative contribution to the echo at the field at which the ENDOR spectrum was recorded. This holds as long as the relaxation times of the two species are comparable and that both have protons in their close environment. Figure 3C shows that in the field range 3.2828–3.4319 the contribution of the minor species is 11–22%. Therefore, it is reasonable to assume that the ENDOR spectrum primarily reflects the major species. Outside this range, on both high and low field edges, the contribution of the minor species is 40% and above; therefore,

these ranges were not included in Figure 4. Figure 4A depicts the ^1H Davies ENDOR spectra of *P. stutzeri* and *P. aeruginosa*

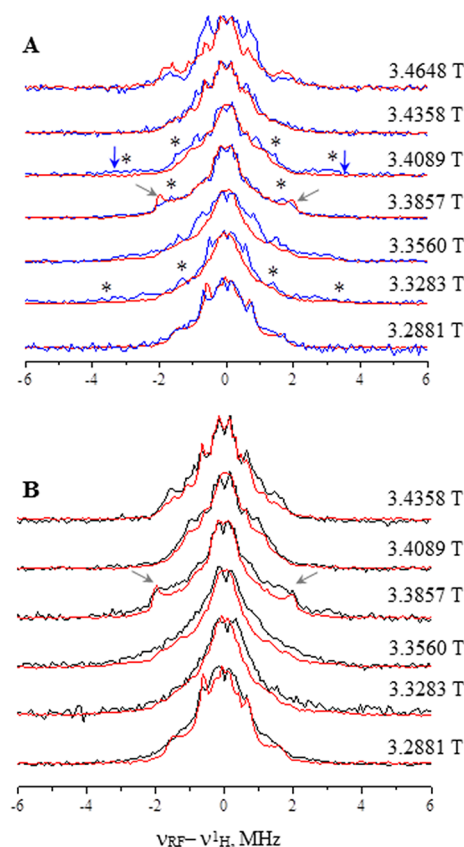


Figure 4. Comparison of the orientation selective ^1H Davies ENDOR spectra of the nitrosyl d_1 -heme complexes of *P. stutzeri* WT-NO (red) with (A) *P. aeruginosa* WT-NO (blue) and (B) *P. aeruginosa* Y10F-NO (black) at the indicated magnetic fields. The large splitting of ~ 8 MHz marked with blue arrows at $B_0 = 3.4089$ T and features marked with asterisk (*) in *P. aeruginosa* WT-NO spectra were previously assigned to $^1\text{H}-\text{O}(\text{Tyr}_{10})$ H-bonded to NO.²⁴ The gray arrows indicate distinct features in the *P. stutzeri* WT-NO spectrum at $B_0 = 3.3857$ T. All spectra were normalized to the most intense signal appearing at the ^1H Larmor frequency.

WT-NO measured at the same magnetic field positions along the EPR powder pattern. Remarkably, the main difference between the two sets is in the features corresponding to the largest splitting, ~ 8 MHz, which are absent in the spectra of *P. stutzeri*. These features are most pronounced at the following field positions: 3.4089 T, 3.3857 T, and 3.3283 T (with corresponding g -values of 1.989, 2.024, and 2.037). A blow-up of the spectra recorded at $B_0 = 3.4089$ T ($g = 1.989$) is shown in Figure S3 in the SI. These features were previously assigned to the H-bonded proton of Tyr_{10} in *P. aeruginosa* WT-NO.²⁴ In addition, *P. stutzeri* WT-NO exhibits distinct features at the $B_0 = 3.3857$ T ($g = 2.002$) spectrum marked with gray arrows in Figure 4. The slight shifts in g_{zz} and g_{yy} values may lead to an inaccurate comparison of the spectra recorded at the same magnetic field because the selected orientations are somewhat different. Accordingly, we also compared the spectra recorded at the principal g -values (see Figure S4, SI) and found that the differences remained significant.

The ^1H ENDOR spectra shown in Figure 4B compare *P. stutzeri* WT-NO with *P. aeruginosa* Y10F-NO. Their high

resemblance throughout the entire field range measured is compelling. Notably, the large coupling, corresponding to H-bonded proton of Tyr₁₀,²⁴ is absent in both *P. stutzeri* WT-NO and *P. aeruginosa* Y10F-NO spectra. This observation is consistent with the fact that *P. stutzeri* WT lacks an equivalent to Tyr₁₀ residue, which is among 26 missing amino acids in its N-terminus. The distinct features of *P. stutzeri* WT-NO marked with gray arrows in the $B_0 = 3.3857$ T ($g = 2.002$) spectrum can be also identified in the *P. aeruginosa* Y10F-NO spectrum recorded at the same field position. These features are probably attributable to one of the conserved histidines¹⁷ in the distal pocket of *P. stutzeri* WT, as proposed previously²⁴ for *P. aeruginosa* Y10F-NO.

²H Mims ENDOR. ²H Mims ENDOR measurements were also performed on samples exchanged with D₂O to determine unambiguously the exchangeable protons in the *P. stutzeri* WT-NO complex. Figure 5A shows a comparison of the spectra of

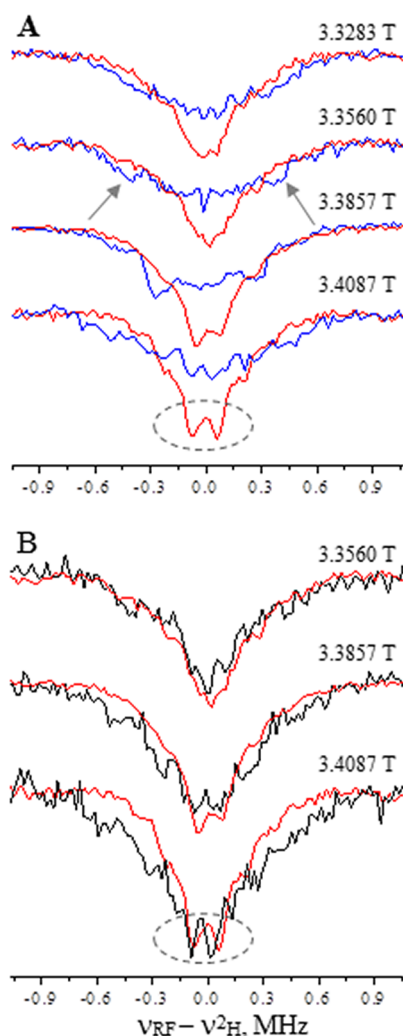


Figure 5. Comparison of orientation selective ²H Mims ENDOR spectra of the nitrosyl d₁-heme complexes of *P. stutzeri* WT-NO (red) with (A) *P. aeruginosa* WT-NO (blue) and (B) *P. aeruginosa* Y10F-NO (black) at the indicated magnetic fields. The spectra were normalized according to the ENDOR effect. The arrows indicate hyperfine coupling of ¹H–O(Tyr₁₀) of *P. aeruginosa* WT-NO. The dashed circles indicate the weakly coupled exchangeable protons, which are present in the nitrosyl d₁-heme complexes of *P. stutzeri* WT-NO and in *P. aeruginosa* Y10F-NO.

P. stutzeri WT-NO and *P. aeruginosa* WT-NO. The comparison of the intensity of the matrix line at the ²H Larmor frequency that reflects interaction with distant solvent molecules and other exchangeable protons is of interest. Therefore, the ENDOR spectra were scaled in this case according to the ENDOR effect, ϵ (see eq 1).

The main difference between the spectra of WT-NO *P. stutzeri* and *P. aeruginosa* is the absence of the large coupling assigned to the H-bonded proton of Tyr₁₀ in the spectrum of *P. stutzeri* WT-NO (see arrows in Figure 5A). This is consistent with its absence in the ¹H ENDOR spectra. In addition, the spectra of *P. stutzeri* WT-NO exhibit much stronger signals close to the ²H Larmor frequency that are marked with circles in Figure 5. These are attributed to distant water molecules. Directly H-bonded water molecules are expected to have substantially larger hyperfine couplings.²⁴ The differences in the ENDOR signal intensity at the ²H Larmor frequency region are very large and unlikely to arise from the minor species with a 11–22% contribution. This strong signal of distant solvent molecules suggests a more open conformation of the d₁-heme distal pocket of the *P. stutzeri* WT-NO compared with the *P. aeruginosa* WT-NO because of the absence of the tyrosine residue. A comparison of the ²H spectra of *P. stutzeri* WT-NO with that of *P. aeruginosa* Y10F-NO, presented in Figure 5B, reveals similar signal intensity at the ²H Larmor frequency for both proteins.

The general similarity between the spectra of *P. stutzeri* WT-NO and *P. aeruginosa* Y10F-NO confirms our earlier identification and characterization of the Tyr₁₀ H-bond to the N(NO) in *P. aeruginosa* WT-NO. The largest hyperfine coupling of an exchangeable proton observed for *P. stutzeri* WT-NO was ~4 MHz, clearly indicating the presence of an H-bond to one (or more) histidine residues, as found for *P. aeruginosa* Y10F-NO.²⁴

¹⁴N HSCORE. Orientation-selective HSCORE measurements were also carried out to substantiate the existence of an axial histidine ligand and to determine the hyperfine coupling of its coordinated nitrogen. Comparison of the obtained values with those reported for nitrosyl complexes of myoglobin (MbNO)²² and *P. aeruginosa* WT-NO²⁴ serves to verify the sensitivity of this hyperfine coupling to changes in the H-bond network in the distal pocket. HSCORE spectra exhibit cross-peaks that represent correlations of all frequencies in one electron spin manifold with those in the other spin manifold. The cross peaks appear at symmetric positions with respect to the diagonal in both the (+, +) and (–, +) quadrants. Figure 6 shows spectra recorded magnetic fields corresponding to $g = 2.054$, $g = 1.972$, and $g = 2.002$. Table 3 lists the observed cross-peak frequencies and their assignments. The spectra are very similar to those observed for *P. aeruginosa* WT-NO (see Figure 6D) and Y10F-NO^{23,24} with the cross peaks practically appearing at the same positions. The peaks on the diagonals are the result of incomplete inversion of the magnetization by the π -pulse. The signals on the (–,+) diagonal are noise. On the basis of this similarity and within the available resolution, we conclude that the coordinated ¹⁴N has the same hyperfine principal values as determined recently for *P. aeruginosa* WT-NO from simulations and DFT calculations.²⁴

DISCUSSION

This study measured and analyzed the properties of the nitrosyl d₁-heme complexes of WT cd₁ NIR from *P. stutzeri* and *P. aeruginosa* of WT and the *P. aeruginosa* Y10F mutant, using

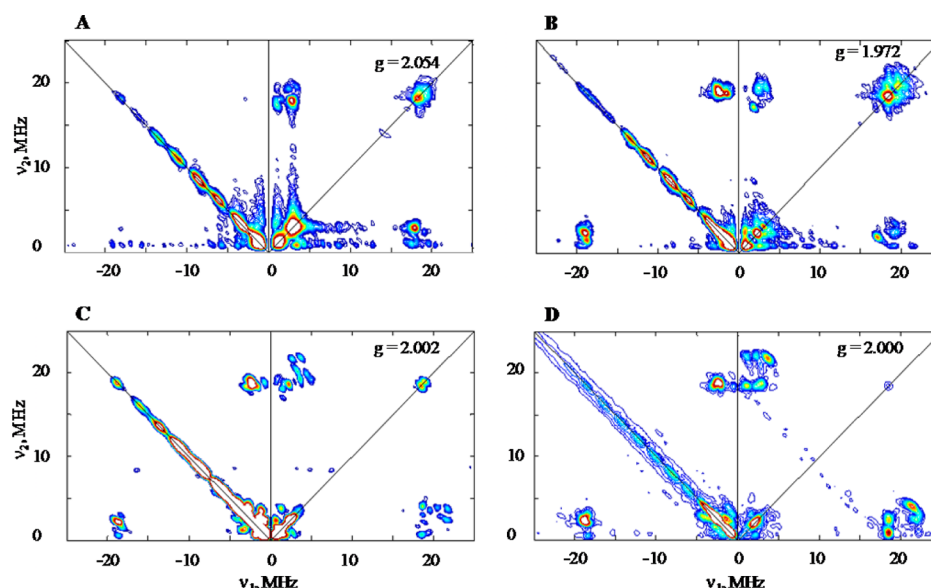


Figure 6. W-band HYSCORE spectra of the nitrosyl d₁-heme of *P. stutzeri* WT-NO (A–C) recorded at magnetic fields corresponding to the g-values listed on the figure, with $\tau = 180$ ns and $\pi/2$ and π pulse lengths of 16 and 32 ns, respectively. (D) The spectrum of the nitrosyl d₁-heme of *P. aeruginosa* WT-NO recorded at $g = 2.000$ with $\pi/2$ of 12.5 ns, π of 25 ns, and $\tau = 220$ ns.

Table 3. HYSCORE Correlation Peaks of *P. stutzeri* WT-NO and Their Assignments

	¹⁴ N _{HIS} cross peak frequencies, MHz	assignment
$g = 1.972$	19.3, 1.4	$\nu_{sq2}^+ \nu_{sq1}^-$
	19.3, 2.3	$\nu_{sq2}^+ \nu_{sq2}^-$
	19.3, 3.5	$\nu_{sq2}^+ \nu_{dq}^-$
	17.1, 1.8	$\nu_{sq1}^+ -$
$g = 2.002$	18.7, 0.8	$\nu_{sq1}^+ \nu_{sq1}^-$
	18.7, 2.3	$\nu_{sq1}^+ \nu_{sq2}^-$
	21.6, 2.4	$\nu_{sq2}^+ \nu_{sq2}^-$
	21.6, 3.9	$\nu_{sq2}^+ \nu_{dq}^-$
$g = 2.054$	17.2, 1.0	$\nu_{sq1}^+ \nu_{sq1}^-$
	18.0, 2.9	
	19.3, 3.4	$\nu_{sq2}^+ \nu_{dq}^-$

pulse EPR techniques at W-band. These techniques were used to gain geometric and electronic structural insights into these enzymes' nitrite reduction site.

Using ¹H/²H ENDOR spectroscopy enabled characterization of the environment of the d₁-heme bound NO ligand of the major species, in particular its H-bond network, and unveiling of structural features previously only hypothesized. The large ¹H hyperfine couplings, observed in the *P. aeruginosa* WT-NO, were found to be missing in *P. stutzeri* WT-NO spectra, as reported previously for the ¹H/²H ENDOR spectra of the *P. aeruginosa* Y10F-NO mutant.²⁴ In our previous study, the absence of the large ¹H hyperfine couplings in *P. aeruginosa* Y10F was the basis for its assignment to the OH proton of Tyr₁₀, which forms an H-bond to N(NO).²⁴ The present results and the fact that *P. stutzeri* cd₁ NIR lacks 26 amino acids in its N-terminus, which includes the equivalent of Tyr₁₀ residue of *P. aeruginosa* cd₁ NIR,¹⁷ strongly substantiate this previous assignment. The comparison also identified H-bonds from one or two of the conserved histidines.

The similar ²H ENDOR spectra of *P. stutzeri* WT-NO and *P. aeruginosa* Y10F-NO are striking and indicate that the nitrosyl d₁-heme distal pocket of both is endowed with a larger solvent exposure than that of *P. aeruginosa* WT-NO.³ The solvent

accessibility is a consequence of the absence of the Tyr in the heme pocket. This phenomenon is in line with the previous suggestions that the solvent accessibility of the d₁-heme pocket is related to the marked differences in the c- to d₁-hemes ET rates between the *P. stutzeri* and *P. aeruginosa* enzymes^{21,45} (see Table 1A,B in ref 21). The faster first step of ET rate in the *P. stutzeri* WT enzyme is characterized by negative activation entropy, whereas its equivalent step in the *P. aeruginosa* WT is enthalpy controlled. Thus, the higher barrier for the ET in the *P. aeruginosa* WT cd₁ NIR is probably related to its undergoing both local and global conformational changes upon electron transfer, which apparently do not take place in the *P. stutzeri* WT enzyme.²¹ A key structural element involved in this ET is the conformational transition of the N-terminus tail, which is absent in *P. stutzeri* cd₁ NIR and that, in the *P. aeruginosa* counterpart, is responsible for the closure of the d₁-heme pocket that decreases solvent accessibility and contributes to the stabilization of the OH[−] axial ligand in the oxidized form.¹⁷ Note that the H369A mutant of *P. aeruginosa* cd₁ NIR also displays an increase in ET rate compared with *P. aeruginosa* WT, and its 3D structure clearly shows a more open d₁-heme pocket and a relocation of the c-heme versus d₁-heme domains.^{16,21} Still, in the absence of both the three-dimensional structure of the *P. stutzeri* WT enzyme and the internal ET rate constant within its Y10F mutant, no conclusions can be reached.²¹

The ¹⁴N hyperfine interactions of the NO and the proximal histidine in the nitrosyl d₁-heme complex of *P. stutzeri* WT were also determined and compared with those of *P. aeruginosa* WT, its Y10F mutant, and the myoglobin nitrosyl complex, MbNO. These results illustrate the sensitivity of the EPR parameters to variations in the heme structure, and distal and proximal residues in nitrosyl heme complexes.

All nitrosyl complexes of d₁-heme (native and mutants) studied at low temperatures exhibited a major species with a highly similar rhombic g-matrix and a minor species with a rhombic symmetry.^{23,24} The presence of multitude of nitrosyl heme complexes in proteins' solutions has been the subject of

interest and debate for several decades. Among these, the case of MbNO has been the most extensively studied. In MbNO solutions, as opposed to crystals,⁴⁶ two species were observed, one with an axial g-tensor and the second with a rhombic g-tensor. The relative amounts of the two species were found to be temperature-dependent.^{47,48} The rhombic species, which prevails at low temperatures, was recently characterized in detail, whereas the axial species remained illusive.²² Recent quantum chemical calculations showed that when the N₃-heme-Fe-N-O dihedral angle is 0° or 180°, the hydrogen bonding interaction of His₆₄ with NO is minimal and allow a rotation of the NO moiety about the Fe-N bond, leading to an axial g.⁴⁹ This study also showed that the g-values are highly sensitive to the dihedral angle mentioned above and the Fe-N-O geometries. Such structural variations are probably the source of the minor species in cd₁ NIR. While the nitrosyl b-heme complexes of myoglobin can have an axial form, the nitrosyl d₁-heme complexes showed only species with rhombic g. This result implies that the rhombicity is a characteristic of the d₁-heme. The absence of an axial form suggests that the energy barrier for a NO rotation is higher in the d₁-heme than in the b-heme of MbNO. Moreover, mutation of key residues in the distal pocket of the d₁-heme of *P. aeruginosa* cd₁ NIR (i.e. His₃₂₇ and His₃₆₉ or Tyr₁₀) caused only very subtle shifts in the g-values of the rhombic species and did not bring about the formation of an axial species in significant amounts.²⁴ Therefore, the removal of these residues does not change the Fe-N-O angle or the Fe-N(NO) bond length because those are expected to have a significant effect on the g-values.^{24,49}

The g_{yy} value of the *P. stutzeri* WT-NO is slightly higher than the corresponding values of *P. aeruginosa* WT-NO, which cannot be attributed to the lack of interaction with a tyrosine residue because the Y10F mutation of this residue did not affect the g-values. In addition, the practically identical ¹⁴N hyperfine coupling of the axial histidine suggests that the Fe-N(His) bond length is similar. These results strongly suggest that the observed difference must be associated with an inherently small diversity in Fe-N-O bond angle or Fe-N(NO) bond length, even though we cannot presently discriminate between these two structural parameters.

Another interesting observation is the invariance of ¹⁴N hyperfine coupling of the coordinated nitrogen of the proximal histidine toward changes in the distal pocket. The ¹⁴N principal hyperfine values in *P. aeruginosa* WT-NO and *P. stutzeri* WT-NO are the same. DFT calculations^{22,24,49} showed that changes in the H-bonding to the NO are expected to affect the spin density distribution among the Fe-N-O atoms, which affects the ¹⁴N hyperfine coupling of the proximal histidine. However, such changes could not be resolved experimentally. The ¹⁴N hyperfine couplings of the proximal histidine in the nitrosyl d₁-heme complexes of cd₁ NIR differ by only ~5% from those of MbNO (see Table 2). Similarly, the ¹⁴N(NO) hyperfine couplings of these two types also differ by a few percent. QM/MM calculations showed that these ¹⁴N hyperfine couplings should be highly sensitive to the Fe-N(O) bond length, the Fe-N-O angle, and the N(por)-Fe-N-O dihedral angle.⁴⁸ Therefore, we suggest that, at least in frozen solutions, these structural elements are close for these two types of proteins. Moreover, the similar electronic properties of the proximal residue agree well with previous data showing that the proximal protein environment does not play a major role in controlling the reactivity of d₁-heme with NO.¹

CONCLUSIONS

The nitrosyl d₁-heme complex of cd₁ NIR from *P. stutzeri* was characterized by W-band pulse EPR techniques and compared with that of *P. aeruginosa*. The dominating species at low temperatures has a rhombic g-tensor and a histidine as proximal ligand. The bonding characteristics of the proximal histidine, as manifested by the ¹⁴N hyperfine couplings, are much the same as in the nitrosyl d₁-heme complex of *P. aeruginosa* cd₁ NIR. The g-values are also similar except for a small change in g_{mid}. The main differences between the nitrosyl d₁-heme complexes are the absence of an H-bond to the N(NO) attributable to the absence of an equivalent to the Tyr₁₀ residue in the N-terminus and the larger solvent accessibility of the d₁-heme pocket of the *P. stutzeri* cd₁ NIR. The latter supports previous suggestions that the faster electron transfer rate from c- to d₁-heme in *P. stutzeri* cd₁ NIR is attributable to an open conformation in the d₁-heme pocket, as suggested by the observed ET activation parameters.²¹

ASSOCIATED CONTENT

Supporting Information

Purification gels, UV-vis, and EPR spectra of the purified cd₁ NIR from *P. stutzeri*. Additional comparison of the orientation selective ¹H Davies ENDOR spectra of the nitrosyl d₁-heme of *P. stutzeri* WT-NO with *P. aeruginosa* WT-NO and Y10F-NO. This material is available free of charge via the Internet at <http://pubs.acs.org>.

AUTHOR INFORMATION

Corresponding Author

*E-mail: Daniella.goldfarb@weizmann.ac.il; phone: +972-8-9342016.

Funding

Funding is by the German-Israel Foundation for Scientific Research.

Notes

The authors declare no competing financial interest.

ACKNOWLEDGMENTS

D.G. holds the Erich Klieger Chair of Chemical Physics. This research was made possible in part by the historic generosity of the Harold Perlman Family. We would like to thank Walter G. Zumft and Peter M. H. Kroneck for initiating the studies on the cd₁ NIR from *P. stutzeri*. We gratefully acknowledge the contribution of Marielle Bauzan (Unité de Fermentation, IMM (Institut de Microbiologie de la Méditerranée)-IFR88-CNRS, Marseilles France) for growing the bacteria.

ABBREVIATIONS USED

cd₁ NIR, cd₁ nitrite reductase; WT, wild type; *P. stutzeri*, *Pseudomonas stutzeri*; *P. aeruginosa*, *Pseudomonas aeruginosa*; EPR, electron paramagnetic resonance; MCD, magnetic circular dichroism; DFT, density functional theory; 3D, three-dimensional; OD, optical density; EDTA, ethylene diamine tetraacetic acid; CW, continuous wave; RF, radio frequency; FS-ED, field swept echo detected; ENDOR, electron-nuclear double resonance; HYSCORE, hyperfine sub level correlation; WT-NO, nitrosyl d₁-heme complex of wild type cd₁ NIR; Y10F-NO, nitrosyl d₁-heme complex of the Y10F mutant of cd₁ NIR; MbNO, nitrosyl heme complex of myoglobin

REFERENCES

- (1) Yamanaka, T., and Okunuki, K. (1963) Crystalline pseudomonas cytochrome oxidase: II. Spectral properties of the enzyme. *Biochim. Biophys. Acta* 67, 394–406.
- (2) Horio, T., Higashi, T., Sasagawa, M., Kusai, K., Nakai, M., and Okunuki, K. (1960) Preparation of crystalline *Pseudomonas* cytochrome c-551 and its general properties. *Biochem. J.* 77, 194–201.
- (3) Nurizzo, D., Silvestrini, M. C., Mathieu, M., Cutruzzolà, F., Bourgeois, D., Fülöp, V., Hajdu, J., Brunori, M., Tegoni, M., and Cambillau, C. (1997) N-terminal arm exchange is observed in the 2.15 Å crystal structure of oxidized nitrite reductase from *Pseudomonas aeruginosa*. *Structure* 5, 1157–1171.
- (4) Allen, J. W. A., Watmough, N. J., and Ferguson, S. J. (2000) A switch in heme axial ligation prepares *Paracoccus pantotrophus* cytochrome cd1 for catalysis. *Nat. Struct. Mol. Biol.* 7, 885–888.
- (5) Zumft, W. G. (1997) Cell biology and molecular basis of denitrification. *Microbiol. Mol. Biol. Rev.* 61, 533–616.
- (6) Silvestrini, M. C., Tordi, M. G., Musci, G., and Brunori, M. (1990) The reaction of *Pseudomonas* nitrite reductase and nitrite. A stopped-flow and EPR study. *J. Biol. Chem.* 265, 11783–11787.
- (7) Averill, B. A. (1996) Dissimilatory Nitrite and Nitric Oxide Reductases. *Chem. Rev.* 96, 2951–2964.
- (8) Rinaldo, S., Brunori, M., and Cutruzzolà, F. (2007) Nitrite controls the release of nitric oxide in *Pseudomonas aeruginosa* cd1 nitrite reductase. *Biochem. Biophys. Res. Commun.* 363, 662–666.
- (9) Kharitonov, V. G., Sharma, V. S., Magde, D., and Koesling, D. (1997) Kinetics of Nitric Oxide Dissociation from Five- and Six-Coordinate Nitrosyl Hemes and Heme Proteins, Including Soluble Guanylate Cyclase. *Biochemistry* 36, 6814–6818.
- (10) Vijgenboom, E., Busch, J. E., and Canters, G. W. (1997) In vivo studies disprove an obligatory role of azurin in denitrification in *Pseudomonas aeruginosa* and show that azu expression in under control of RpoS and ANR. *Microbiology* 143, 2853–2863.
- (11) Rinaldo, S., Sam, K. A., Castiglione, N., Stelitano, V., Arcovito, A., Brunori, M., Allen, J. W., Ferguson, S. J., and Cutruzzolà, F. (2011) Observation of fast release of NO from ferrous d1 haem allows formulation of a unified reaction mechanism for cytochrome cd1 nitrite reductases. *Biochem. J.* 435, 217–225.
- (12) Nurizzo, D., Cutruzzolà, F., Arese, M., Bourgeois, D., Brunori, M., Cambillau, C., and Tegoni, M. (1998) Conformational Changes Occurring upon Reduction and NO Binding in Nitrite Reductase from *Pseudomonas aeruginosa*. *Biochemistry* 37, 13987–13996.
- (13) Fülöp, V., Moir, J. W. B., Ferguson, S. J., and Hajdu, J. (1995) The anatomy of a bifunctional enzyme: Structural basis for reduction of oxygen to water and synthesis of nitric oxide by cytochrome cd1. *Cell* 81, 369–377.
- (14) Cutruzzolà, F., Brown, K., Wilson, E. K., Bellelli, A., Arese, M., Tegoni, M., Cambillau, C., and Brunori, M. (2001) The nitrite reductase from *Pseudomonas aeruginosa*: Essential role of two active-site histidines in the catalytic and structural properties. *Proc. Natl. Acad. Sci. U. S. A.* 98, 2232–2237.
- (15) Cutruzzolà, F., Arese, M., Grasso, S., Bellelli, A., and Brunori, M. (1997) Mutagenesis of nitrite reductase from *Pseudomonas aeruginosa*: tyrosine-10 in the c heme domain is not involved in catalysis. *FEBS Lett.* 412, 365–369.
- (16) Brown, K., Roig-Zamboni, V., Cutruzzolà, F., Arese, M., Sun, W., Brunori, M., Cambillau, C., and Tegoni, M. (2001) Domain Swing Upon His to Ala Mutation in Nitrite Reductase of *Pseudomonas aeruginosa*. *J. Mol. Biol.* 312, 541–554.
- (17) Jüngst, A., Wakabayashi, S., Matsubara, H., and Zumft, W. G. (1991) The nirSTBM region coding for cytochrome cd1-dependent nitrite respiration of *Pseudomonas stutzeri* consists of a cluster of mono-, di-, and tetraheme proteins. *FEBS Lett.* 279, 205–209.
- (18) Silvestrini, M. C., Galeotti, C. L., Gervais, M., Schininà, E., Barra, D., Bossa, F., and Brunori, M. (1989) Nitrite reductase from *Pseudomonas aeruginosa*: Sequence of the gene and the protein. *FEBS Lett.* 254, 33–38.
- (19) Smith, G. B., and Tiedje, J. M. (1992) Isolation and characterization of a nitrite reductase gene and its use as a probe for denitrifying bacteria. *Appl. Environ. Microbiol.* 58, 376–384.
- (20) Cheesman, M. R., Ferguson, S. J., Moir, J. W. B., Richardson, D. J., Zumft, W. G., and Thomson, A. J. (1997) Two Enzymes with a Common Function but Different Heme Ligands in the Forms as Isolated. Optical and Magnetic Properties of the Heme Groups in the Oxidized Forms of Nitrite Reductase, Cytochrome cd1, from *Pseudomonas stutzeri* and *Thiosphaera pantotropha*. *Biochemistry* 36, 16267–16276.
- (21) Farver, O., Kroneck, P. M. H., Zumft, W. G., and Pecht, I. (2002) Intramolecular electron transfer in cytochrome cd1 nitrite reductase from *Pseudomonas stutzeri*; kinetics and thermodynamics. *Biophys. Chem.* 98, 27–34.
- (22) Farver, O., Brunori, M., Cutruzzolà, F., Rinaldo, S., Wherland, S., and Pecht, I. (2009) Intramolecular Electron Transfer in *Pseudomonas aeruginosa* cd1 Nitrite Reductase: Thermodynamics and Kinetics. *Biophys. J.* 96, 2849–2856.
- (23) Radoul, M., Sundararajan, M., Potapov, A., Riplinger, C., Neese, F., and Goldfarb, D. (2010) Revisiting the nitrosyl complex of myoglobin by high-field pulse EPR spectroscopy and quantum mechanical calculations. *Phys. Chem. Chem. Phys.* 12, 7276–7289.
- (24) Radoul, M., Centola, F., Rinaldo, S., Cutruzzolà, F., Pecht, I., and Goldfarb, D. (2009) Heme d1 Nitrosyl Complex of cd1 Nitrite Reductase Studied by High-Field-Pulse Electron Paramagnetic Resonance Spectroscopy. *Inorg. Chem.* 48, 3913–3915.
- (25) Radoul, M., Bykov, D., Rinaldo, S., Cutruzzolà, F., Neese, F., and Goldfarb, D. (2011) Dynamic Hydrogen-Bonding Network in the Distal Pocket of the Nitrosyl Complex of *Pseudomonas aeruginosa* cd1 Nitrite Reductase. *J. Am. Chem. Soc.* 133, 3043–3055.
- (26) Weeg-Aerssens, E., Wu, W. S., Ye, R. W., Tiedje, J. M., and Chang, C. K. (1991) Purification of cytochrome cd1 nitrite reductase from *Pseudomonas stutzeri* JM300 and reconstitution with native and synthetic heme d1. *J. Biol. Chem.* 266, 7496–7502.
- (27) Coyle, C. L., Zumft, W. G., Kroneck, P. M. H., Körner, H., and Jakob, W. (1985) Nitrous oxide reductase from denitrifying. *Eur. J. Biochem.* 153, 459–467.
- (28) Parr, S. R., Barber, D., and Greenwood, C. (1976) A purification procedure for the soluble cytochrome oxidase and some other respiratory proteins from *Pseudomonas aeruginosa*. *Biochem. J.* 157, 423–430.
- (29) Arese, M., Zumft, W. G., and Cutruzzolà, F. (2003) Expression of a fully functional cd1 nitrite reductase from *Pseudomonas aeruginosa* in *Pseudomonas stutzeri*. *Protein Expr. Purif.* 27, 42–48.
- (30) Minagawa, N., and Zumft, W. G. (1988) Cadmium-copper antagonism in the activation of periplasmic nitrous oxide reductase of copper-deficient cells from *Pseudomonas stutzeri*. *BioMetals* 1, 117–122.
- (31) van Wonderen, J. H., Knight, C., Oganessian, V. S., George, S. J., Zumft, W. G., and Cheesman, M. R. (2007) Activation of the Cytochrome cd1 Nitrite Reductase from *Paracoccus pantotrophus*. Reaction of oxidized enzyme with substrate drives a ligand switch at heme c. *J. Biol. Chem.* 282, 28207–28215.
- (32) Johnson, M. K., Thomson, A. J., Walsh, T. A., Barber, D., and Greenwood, C. (1980) Electron paramagnetic resonance studies on *Pseudomonas* nitrosyl nitrite reductase. Evidence for multiple species in the electron paramagnetic resonance spectra of nitrosyl haemoproteins. *Biochem. J.* 189, 285–294.
- (33) Goldfarb, D., Lipkin, Y., Potapov, A., Gorodetsky, Y., Epel, B., Raitsimring, A. M., Radoul, M., and Kaminker, I. (2008) HYSCORE and DEER with an upgraded 95 GHz pulse EPR spectrometer. *J. Magn. Reson.* 194, 8–15.
- (34) Stoll, S., and Schweiger, A. (2006) EasySpin, a comprehensive software package for spectral simulation and analysis in EPR. *J. Magn. Reson.* 178, 42–55.
- (35) http://www.boep.specman4epr.com/kv_intro.html.
- (36) Davies, E. R. (1974) A new pulse endor technique. *Phys. Lett. A* 47, 1–2.
- (37) Mims, W. B. (1965) Pulsed Endor Experiments. *Proc. R. Soc. London Series A* 283, 452–457.

- (37) Epel, B., Arieli, D., Baute, D., and Goldfarb, D. (2003) Improving W-band pulsed ENDOR sensitivity—random acquisition and pulsed special TRIPL. *J. Magn. Reson.* 164, 78–83.
- (38) Höfer, P., Grupp, A., Nebenführ, H., and Mehring, M. (1986) Hyperfine sublevel correlation (hyscore) spectroscopy: a 2D ESR investigation of the squaric acid radical. *Chem. Phys. Lett.* 132, 279–282.
- (39) Cutruzzolà, F. (1999) Bacterial nitric oxide synthesis. *Biochim. Biophys. Acta (BBA) - Bioenergetics* 1411, 231–249.
- (40) Silvestrini, M. C., Falcinelli, S., Ciabatti, I., Cutruzzolà, F., and Brunori, M. (1994) *Pseudomonas aeruginosa* nitrite reductase (or cytochrome oxidase): An overview. *Biochimie* 76, 641–654.
- (41) Das, T. K., Wilson, E. K., Cutruzzola, F., Brunori, M., and Rousseau, D. L. (2001) Binding of NO and CO to the d1 Heme of cd1 Nitrite Reductase from *Pseudomonas aeruginosa*. *Biochemistry* 40, 10774–10781.
- (42) Calmels, S., Ohshima, H., Henry, Y., and Bartsch, H. (1996) Characterization of bacterial cytochrome cdt-nitrite reductase as one enzyme responsible for catalysis of nitrosation of secondary Amines. *Carcinogenesis* 17, 533–536.
- (43) Silvestrini, M. C., Colosimo, A., Brunori, M., Walsh, T. A., Barber, D., and Greenwood, C. (1979) A re-evaluation of some basic structural and functional properties of *Pseudomonas* cytochrome oxidase. *Biochem. J.* 183, 701–709.
- (44) LoBrutto, R., Wei, Y. H., Mascarenhas, R., Scholes, C. P., and King, T. E. (1983) Electron nuclear double resonance and electron paramagnetic resonance study on the structure of the NO-ligated heme alpha 3 in cytochrome c oxidase. *J. Biol. Chem.* 258, 7437–7448.
- (45) Farver, O., Kroneck, P. M. H., Zumft, W. G., and Pecht, I. (2003) Allosteric control of internal electron transfer in cytochrome cd(1) nitrite reductase. *Proc. Nat. Acad. Sci. USA* 100, 7622–7625.
- (46) Copeland, D. M., Soares, A. S., West, A. H., and Richter-Addo, G. B. (2006) Crystal structures of the nitrite and nitric oxide complexes of horse heart myoglobin. *J. Inorg. Biochem.* 100, 1413–1425.
- (47) Morse, R. H., and Chan, S. I. (1980) Electron-paramagnetic resonance studies of nitrosyl ferrous heme complexes- determination of an equilibrium between two conformations. *J. Biol. Chem.* 255, 7876–7882.
- (48) Schmidt, P. P., Kappl, R., and Hüttermann, J. (2001) On the mode of hexacoordinated NO-Binding to myo- and hemoglobin: Variable-temperature EPR studies at multiple microwave frequencies. *Appl. Magn. Reson.* 21, 423–440.
- (49) Sundararajan, M., and Neese, F. (2012) Detailed QM/MM study of the Electron Paramagnetic Resonance Parameters of Nitrosyl Myoglobin. *J. Chem. Theory Comput.* 8, 563–574.